

This article was downloaded by: [KSU Kent State University]

On: 20 August 2015, At: 07:54

Publisher: Taylor & Francis

Informa Ltd Registered in England and Wales Registered Number: 1072954 Registered office: 5 Howick Place, London, SW1P 1WG



## Liquid Crystals

Publication details, including instructions for authors and subscription information:

<http://www.tandfonline.com/loi/tlct20>

### Analysis of surface anchored lattice plane orientation in blue phase liquid crystal and its in-plane electric field-dependent capacitance response

Prasenjit Nayek<sup>a</sup>, No Hyun Park<sup>b</sup>, Seong Cheol Noh<sup>b</sup>, Seung Hee Lee<sup>b</sup>, Heung Shik Park<sup>c</sup>, Hyuck Jin Lee<sup>c</sup>, Chien-Tsung Hou<sup>d</sup>, Tsung-Hsien Lin<sup>d</sup> & Hiroshi Yokoyama<sup>e</sup>

<sup>a</sup> Department of Ophthalmology and Visual Science, The Ohio State University, Columbus, USA

<sup>b</sup> Applied Materials Institute for BIN Convergence, Department of BIN Fusion Technology and Department of Polymer-Nano Science and Technology, Chonbuk National University, Jeonju, Republic of Korea

<sup>c</sup> Samsung Displays Co, Giheung, Republic of Korea

<sup>d</sup> Department of Photonics, National Sun Yat Sen University, Kaohsiung, Taiwan

<sup>e</sup> Liquid Crystal Institute, Kent State University, Kent, USA

Published online: 25 Jun 2015.



[Click for updates](#)

To cite this article: Prasenjit Nayek, No Hyun Park, Seong Cheol Noh, Seung Hee Lee, Heung Shik Park, Hyuck Jin Lee, Chien-Tsung Hou, Tsung-Hsien Lin & Hiroshi Yokoyama (2015) Analysis of surface anchored lattice plane orientation in blue phase liquid crystal and its in-plane electric field-dependent capacitance response, *Liquid Crystals*, 42:8, 1111-1119, DOI: [10.1080/02678292.2015.1025874](https://doi.org/10.1080/02678292.2015.1025874)

To link to this article: <http://dx.doi.org/10.1080/02678292.2015.1025874>

PLEASE SCROLL DOWN FOR ARTICLE

Taylor & Francis makes every effort to ensure the accuracy of all the information (the "Content") contained in the publications on our platform. However, Taylor & Francis, our agents, and our licensors make no representations or warranties whatsoever as to the accuracy, completeness, or suitability for any purpose of the Content. Any opinions and views expressed in this publication are the opinions and views of the authors, and are not the views of or endorsed by Taylor & Francis. The accuracy of the Content should not be relied upon and should be independently verified with primary sources of information. Taylor and Francis shall not be liable for any losses, actions, claims, proceedings, demands, costs, expenses, damages, and other liabilities whatsoever or howsoever caused arising directly or indirectly in connection with, in relation to or arising out of the use of the Content.

This article may be used for research, teaching, and private study purposes. Any substantial or systematic reproduction, redistribution, reselling, loan, sub-licensing, systematic supply, or distribution in any form to anyone is expressly forbidden. Terms & Conditions of access and use can be found at <http://www.tandfonline.com/page/terms-and-conditions>

## Analysis of surface anchored lattice plane orientation in blue phase liquid crystal and its in-plane electric field-dependent capacitance response

Prasenjit Nayek<sup>a</sup>, No Hyun Park<sup>b</sup>, Seong Cheol Noh<sup>b</sup>, Seung Hee Lee<sup>b\*</sup>, Heung Shik Park<sup>c</sup>, Hyuck Jin Lee<sup>c</sup>, Chien-Tsung Hou<sup>d</sup>, Tsung-Hsien Lin<sup>d\*</sup> and Hiroshi Yokoyama<sup>e</sup>

<sup>a</sup>Department of Ophthalmology and Visual Science, The Ohio State University, Columbus, USA; <sup>b</sup>Applied Materials Institute for BIN Convergence, Department of BIN Fusion Technology and Department of Polymer-Nano Science and Technology, Chonbuk National University, Jeonju, Republic of Korea; <sup>c</sup>Samsung Displays Co, Giheung, Republic of Korea; <sup>d</sup>Department of Photonics, National Sun Yat Sen University, Kaohsiung, Taiwan; <sup>e</sup>Liquid Crystal Institute, Kent State University, Kent, USA

(Received 27 January 2015; accepted 2 March 2015)

Uniformly oriented macroscopic monodomain of cholesteric blue phase liquid crystal has been realised by the influence of surface anchoring. Orientation of the lattice planes in surface-treated (ST) and non-surface-treated (NST) cell were analysed and compared by Kossel diagram technique. NST cell has revealed the green and blue domains corresponding to reflection from oriented (110) and (112) planes of the body-centred cubic lattice. However, in the ST cell only the lattice plane (110) oriented uniformly and tailored the macroscopic monodomain. Electric field driven reorientation of the (110) lattice plane was noticed in NST cell whereas for ST cell such reorientation was absent. Two distinct electric field-induced capacitive responses have been observed in the two different cells. In NST cell anomalous electrostriction was observed, whereas for ST cell normal electrostriction was observed. Interestingly, the capacitance has decreased with an increasing electric field for anomalous electrostriction in NST cell, whereas for normal electrostriction in ST cell it was increased with increasing the field. Such a capacitive change behaviour is explained by dielectric anisotropic change followed by the electric field induced elongation and contraction of the cubic unit cell along and perpendicular to the electric field.

**Keywords:** blue phase liquid crystal; electrostriction; capacitive response liquid crystal display

### 1. Introduction

A phenomenal example of soft matter in which networks of defects and disclination lines are self-assembled as a fully periodic three-dimensional structure is blue phase liquid crystal (BPLC).[1] Among three types of stable BPLCs BP I has a body-centred cubic (bcc) structure whereas BP II has simple cubic structure (sc).[2] The BP I director field possesses the symmetry group  $O^8$  (I4<sub>1</sub>32) and BP II,  $O^2$  (P4<sub>2</sub>32).[2] The symmetry of BP III phase is the same as that of the isotropic phase.[3–6] In general BPs arise in a narrow temperature range between isotropic and chiral nematic (N\*) phase. Recently, BPLC has been applied to liquid crystal displays and its sub-millisecond order response time could be helpful to construct a more realistic moving image quality with unprecedented high image-driving speed without any overdrive circuit.[7] A fast grey-to-grey response time [8] minimises blurring in the motion-image blur and enables field-sequential-colour displays without colour filters if a set of red, green, blue light emitting diode (LED) backlight is used. The transmittance of BPLC is insensitive to the cell gap as long as it exceeds 2–3  $\mu\text{m}$ . [9] This cell gap insensitivity is mainly advantageous for large panel liquid crystal displays

(LCDs) from the perspective of manufacturing yield. Nevertheless, due to lack of wide thermal stability, it suffers from practical applications such as displays, soft photonic lasers, lenses, switches etc. Different authors have tried to address the problem of thermal stability of BPs by different techniques, i.e., Kikuchi et al. [10] reported the polymer-stabilised BP (PSBP) by creating polymer networks at the site of disclination lines whereas Castles et al. [11] showed another technique by producing template by polymerisation. Nanoparticle induced stabilisation was also proposed and tried experimentally by different authors.[12–15] In addition to these attempts, direct approaches to synthesise BPLCs have also been taken to get wide range BPs.[16,17] It is possible to overcome the high driving voltage by using protruded electrodes [18] and wall-shaped electrodes.[19] The low contrast ratio due to residual birefringence and hysteresis are the impediments that have to be overcome in commercialisation.[20,21] Chen et al. [22] showed that pristine BP II has negligible hysteresis compared to pristine BP I. Nevertheless, polymerised BP I and BP II both suffer from hysteresis. In our earlier report Mukherjee et al. [23] have reported an optically isotropic, transient state by addressing the cell with a low frequency

\*Corresponding authors. Email: [lsh1@chonbuk.ac.kr](mailto:lsh1@chonbuk.ac.kr) and [jameslin@faculty.nsysu.tw](mailto:jameslin@faculty.nsysu.tw)

square wave electric field. The hysteresis of that state was improved significantly but it was due to ionic origin. Hysteresis also seems to be dependent on the grain size.[24] Our recent report showed that a mono domain could be obtained by surface treatment of the cell that effectively reduces the hysteresis but detailed mechanism has not been studied.[25] There is a profound impact of crystal orientation and packing of the nano-sized cubes (unit cell size few hundred nanometres) on the hysteresis, operating voltage, and contrast ratio of BPCL displays (BPLCDs).

In this paper we have studied extensively the detailed mechanism of the surface treatment effect and how it constrains the growth and orientation and packing of the nano-cubes compared to non-surface-treated cells. Also we have measured and compared the contrast ratio between the ST and NST cell. We have tried to analyse the orientation of lattice planes by measuring the reflectance and Kossel diagrams.[26–28] We have found an analogy of electroactive capacitance change which is analogous to the normal and anomalous electrostriction depending on the crystal orientation with respect to the electric field direction.[29] In normal electrostriction (BPI,  $\Delta\epsilon > 0$ ) when an electric field is applied along twofold axes of the cube, the unit cell dimension increases along the electric field and thus capacitance also increases in a similar way with electric field. When electric field acts along the fourfold axes of the cubic unit cell, the size of the unit cell along the electric field decreases and capacitance also varies in a similar way. This analogy could be helpful for the detection of normal and anomalous electrostriction in cubic BPI ( $\Delta\epsilon > 0$ ), under in-plane electric field geometry. Capacitance increases as temperature decreases in ST and NST cells which might be due to temperature dependent cubic unit cell dimension increase as confirmed by temperature dependent Kossel diagram. It is worthy to say that in nematic LC, the capacitance increases with decreasing temperature because ordering of LC increases with decreasing temperature. The temperature dependent capacitance can help to find in situ detection of different BP phase sequence under in-plane cell geometry.

## 2. Experiments

Commercially available BPLC, LCMS-BP-081009-1 (LC Matter Corporation, USA), which consists of the host nematic liquid crystal (NLC) mixture of cyanobiphenyl and cyanoterphenyl group was used. The isotropic-to-BP I transition took place at 66.6°C and the BP I-to-chiral nematic transition was observed at 63°C during cooling in the NST cell. The host NLCs have dielectric anisotropy ( $\Delta\epsilon$ ) of + 14–17 and

birefringence ( $\Delta n$ ) = 0.25–0.28 at 589 nm which are mixed with chiral dopants ZLI4572 (8 wt%) and CB15 (22 wt%). In order to observe field-induced LC reorientation and electro-optic measurements, interdigitated electrodes with its width ( $w$ ) and the distance ( $l$ ) of 4  $\mu\text{m}$  is used and the cell gap between two substrates is 5  $\mu\text{m}$ . Surface treatment was performed by coating the inner surfaces of the glass substrates with commercially available planar polyimide with thickness of 1000 Å. These PI layers are mechanically buffed to produce uniform azimuthal anchoring with low pretilt angle. Top and bottom electrodes are rubbed in antiparallel direction. The textures of BPLC were taken by using a polarising optical microscope (POM), with Nikon microscope fitted with a DXM1200 camera. The cooling rate of the LC cells was controlled using a temperature controller (Linkam, TMS 94, Tadworth, UK) at 0.1°C/min. The cell has been driven with variable amplitude, square wave pulse with a frequency of 1 kHz from a function generator (Tektronix, AFG3022, Beaverton, OR, USA) connected to an amplifier. The capacitance measurement has been performed by an Agilent 4284A precision LCR metre (20–1000 kHz). For reflectance measurement we have used USB 2000+ spectrometer from Ocean Optics. Kossel diagram was observed by the POM image in the reflection mode due to the Bragg type reflection from the different plane orientation when the sample was illuminated by monochromatic light.

## 3. Results and discussion

The POM textures of the blue and green domains of the NST cell are depicted in Figure 1(a) and 1(c), respectively. Corresponding Kossel diagram for blue domain and green domains are depicted in Figure 1(b) and 1(d), respectively. Careful Kossel analysis has revealed that blue and green domains are corresponding to the reflection from planes of (112) and (110). The unit cell orientations on the substrate decorated by in-plane electrodes are schematically represented in Figure 1(e). Capacitance vs. voltage ( $C$ – $V$ ) variations at different temperatures are shown in Figure 1(f). Each  $C$ – $V$  curve shows two steps, one is in the low voltage (0–5 V) and another step is in the higher voltage side (>5–6 V up to 15 V). Interestingly, we can see that capacitance decreases with increasing voltage amplitude. It is also noteworthy that capacitance of the cell increases with decreasing temperature. As it is well known that for BP I, when temperature decreases the pitch or the unit cell dimension increases that could manifest increase in the capacitance. Temperature dependent  $C$ – $V$  curve reflects that there may be some relation between

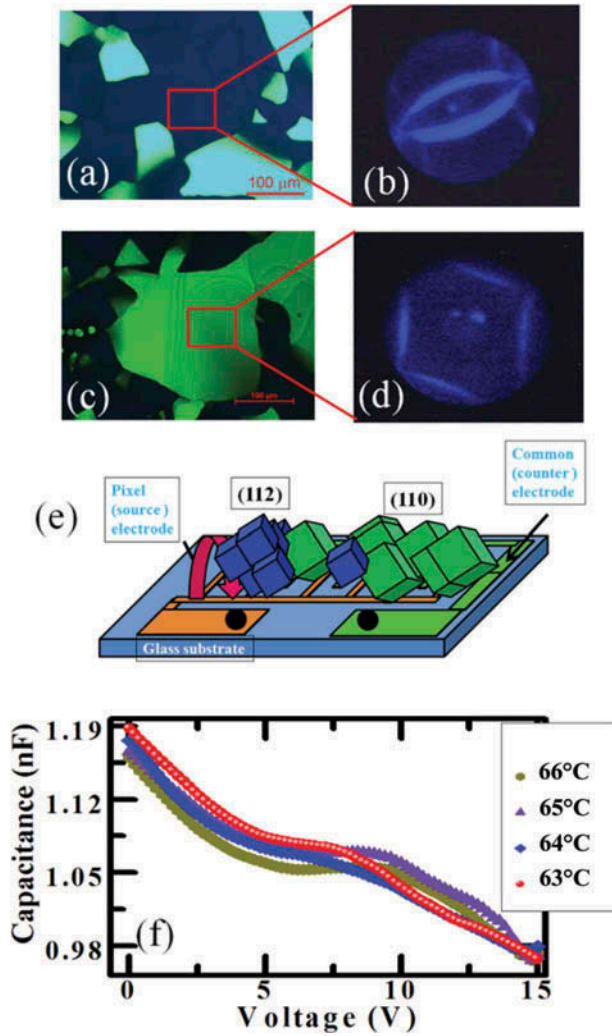


Figure 1. NST cell at 66°C: (a) blue and green domain texture in reflection mode (blue domain shown by red square), (b) Kossel diagram, corresponding to blue domain when the sample was illuminated by a monochromatic light of wavelength 440 nm, in which the blue domain corresponds to the reflection from (112) plane of BPI, (c) green domain texture, (d) corresponding Kossel diagram, when the sample was illuminated by a monochromatic light of wavelength 440 nm in which green domain corresponds to (110) plane, (e) the schematic diagram of the orientation of the nanoscopic cubic unit cells, in which green and blue corresponds to the orientation of (110) and (112) plane, respectively, along the viewing direction, (f) capacitance (C) vs. voltage (V) for different temperatures at driving frequency of 1 kHz.

decrease in capacitance and shrinkage of cubic unit cell along the electric field. Figure 2(a) shows the reflectance with respect to wavelength of an incident light for different voltages for the green domain i.e. (110) plane. It is quite clear that initially (<10 V) there is only one reflection peak due to (110) reflection

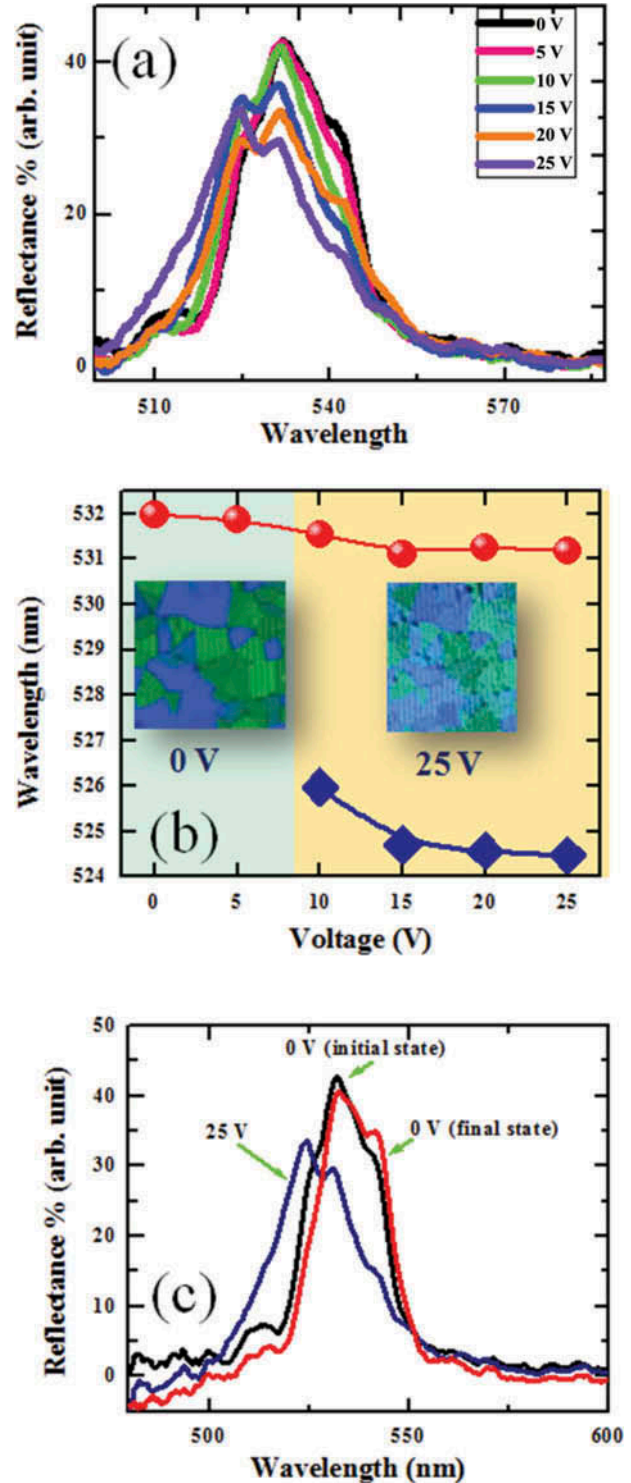


Figure 2. (a) Reflection spectrum for NST and IPS cell with different voltages, (b) reflection peak wavelength vs. voltage (red circle is corresponding to (110) plane reflection and the other is from (100) plane, in which inset picture shows the textures corresponding to the 0 V and 25 V), (c) Reflectance corresponding to 0 V, 25 V and again to 0 V.

peak. At about 10 V there is a fragmentation in the reflection peak followed by a slight blue shift (for higher wavelength side peak) and then remains constant for further increase in voltage. The fragmentation of the (110) spectral line has been attributed to the dual origin, first is reorientation of the (110) plane by electric field and second is new plane arising due to departure from the initial cubic lattice structure due to electrostriction. From 0 to 5 V, the (110) plane reflection wavelength slightly decreases (Figure 2(b), red circle), and it might be due to the reorientation of the cubic lattice plane as a consequence of reorientation of the LCs inside the double twisted cylinder. With further increase of voltage, wavelength decreases slightly, which might be due to reorientation of the (110) plane under in-plane electric field, as it is not exactly along the direction of (110) plane. The reason behind the reorientation of cubic unit cell may be due to electrical torque acting by the in-plane electric field. The reorientation of the cubic unit cell is easier in NST cell because blue and green domains coexist and grains are not densely packed due to lattice mismatch. This reorientation causes the blue shift in the region  $>5$  V (Figure 2(b), red circle). Reflection amplitude decreases, with increasing voltage, indicating that (110) plane is reorienting so that reflection is lacking from that particular plane. Second peak (Figure 2(b), blue colour, lower wavelength side peak) shows prominent blue shift with increasing voltages and saturates at higher voltages. Reflection amplitude increases, with increasing voltage, an extra plane arises through structural deformation of the bcc lattice to tetragonal lattice.[30–32] The second splitting is probably due to Bragg reflection from fourfold (100) axis, parallel to the electric field. As reported by Heppke et al. [29] that fourfold axis parallel to the surface normal not only reflects light from (100) or (200) plane but also from (110) plane, so we are assuming that fourfold axis is parallel to the electric field. In agreement with the above reference we are getting two reflection peaks, one is from (110) and another should be from (100). The lattice size decreases as electric field increases parallel to (100) axis and blue shift has occurred. Figure 2(c) shows that when voltage is withdrawn after application of 25 V, the structure is not completely restored, which might be due to lattice deformation which is also predicted by theoretical computational result.[33] This deformed structure under strong electric field induces the residual birefringence which is an impediment of device construction. We will discuss later how to avoid this by avoiding overdrive which also reduces the hysteresis. The POM texture for the ST cell with different temperature is demonstrated in Figure 3(a). The Kossel diagram of the monodomain blue phase

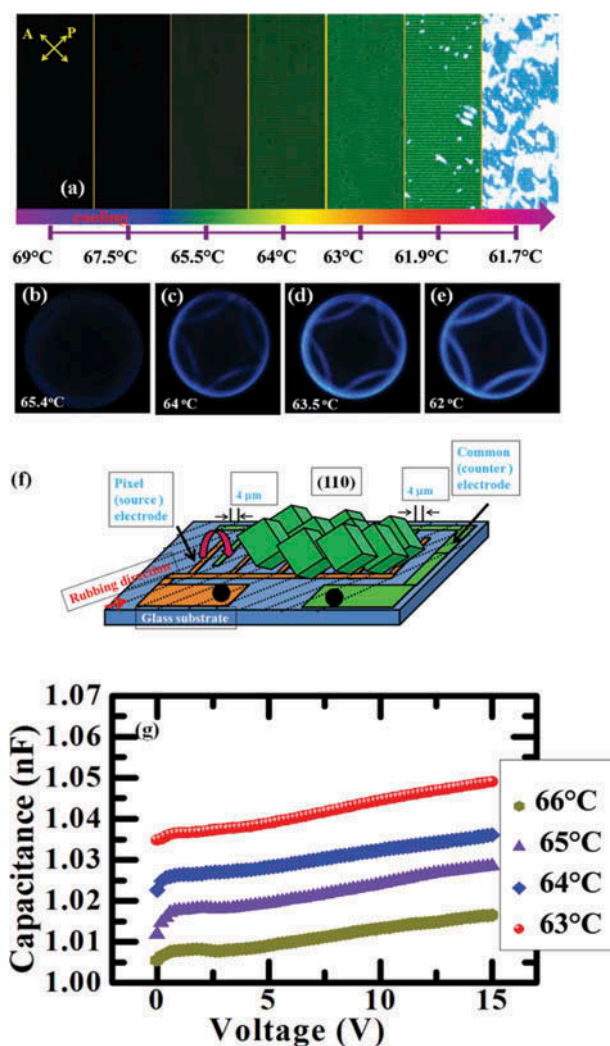


Figure 3. (a) Texture for ST cell for different temperatures, at 69°C (texture is black due to isotropic phase), at 61.9°C (white light leakage is due to transition from BP to N\*), (b)–(e) Kossel diagram by a monochromatic light of wavelength 514 nm shown at different temperatures, (f) schematic diagram of the orientation of the nanocubes in ST cell, (g)  $C$ – $V$  for different temperatures at 1 kHz.

at different temperatures is shown in Figure 3(b) and 3(e). The Kossel diagram pattern shows the (110) planes are along the viewing direction. Strong anchoring force of the PI type of alignment material helps to orient the (110) planes into macroscopic domain so that the texture is uniform. The arrangement of the unit cell which is of several nanometre orders is schematically illustrated in Figure 3(f). Figure 3(g) shows the  $C$ – $V$  curve for the ST cell. Dramatically, we have observed the opposite result for ST cell that capacitance increases with increasing voltages. This might be due to expansion of the cubic unit cell along the electric field. Figure 4 shows the reflectivity as a

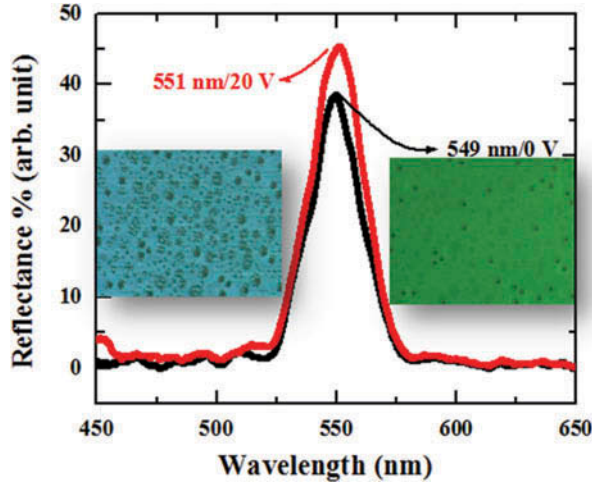


Figure 4. (colour online) Reflectance vs. wavelength for ST cell for 0 and 25 V.

function wavelength (nm) of an incident light for ST cell. Black spectrum is for 0 V and red one is for 20 V. We can see that for 20 V the peak of the spectrum red shifted which indicates that electric field acts almost parallel to the twofold axis so unit cell elongation took place and red shift occurred. Also orientation of the unit cell as occurred for NST cell has been prohibited due to compact packing of the unit cell as illustrated in Figure 3(f). Weak electric fields cause the deformation of the unit cell proportional to the square of the electric field.[34–36] In the low electric field limit, these deformations are expressed by the electrostriction tensor  $\mathbf{R}$ . Under small field strengths the electrostriction may be described by

$$u_{ij}(E) = R_{ijkl}E_kE_l \quad (1)$$

where  $u_{ij} = \frac{1}{2}(\partial_i u_j + \partial_j u_i)$  is the symmetric deformation tensor and  $R_{ijkl}$  is the component of the electrostriction tensor. If we consider three independent components, namely,  $R_1 \equiv R_{xxxx}$ ,  $R_2 \equiv R_{xyxy}$  and  $R_3 \equiv 2R_{yzzy}$ . If  $R_1/R_3 < 0$  for BPI ( $\Delta\epsilon > 0$ ), the corresponding electrostriction is called anomalous electrostriction. In anomalous electrostriction (for BPI and  $\Delta\epsilon > 0$ ), a contraction of the unit cell is seen when the electric field is applied parallel to the fourfold axis of the cube whereas, an expansion took place for fields parallel to twofold axis. It is clear from Figure 2(a) and 2(b) that for NST cell, wavelength decreases with increasing voltages similar to  $C-V$  graph. Decrease in wavelength with increasing voltage indicates a blue shift, indicating that the lattice spacing decreases with voltage. On the other hand we can say that length of the unit cell decreases along the electric field, indicating anomalous electrostriction took place as a

consequence, capacitance also decreases with increasing electric field. This happens when fourfold axis is parallel to the electric field. In NST cell as voltage induced twofold (110) direction of the bcc lattice transformed to the fourfold (100) direction of the tetragonal lattice. This is evident from Figure 2(b) as new peak towards low wavelength side arises such that (100) direction also reorients slightly along the in-plane electric field acting along (100) plane and then contraction of the unit cell took place. On the other hand ST cell's wavelength shifts towards higher wavelength side, indicating that pitch increases along the electric field (cube expands along the electric field direction) so capacitance increases. This happens when twofold axes is parallel to the applied electric field for BPI phase and host LC has a positive  $\Delta\epsilon$ . Now we will calculate the electro-active deformation of the unit cell and compare the results with the changes of the capacitance of both the test cells. Here we would like to show that theoretical calculation of the distortion of the unit cell is proportional to the changes of capacitance in either case, meaning that if electric field is parallel to the twofold or fourfold axis changes in capacitance follows the contraction or elongation of the unit cell. In other words, if unit cell increases along the electric field direction then capacitance increases and vice versa. We will now discuss the case when the applied electric field is parallel to the fourfold axis (e.g.,  $E \parallel [100]$ ). In NST cell in-plane electric field orients [100] axis parallel to the electric field. So it is logical to consider the case, Figure 5(a) [inset,  $E = 0$ ] where it is shown that electric field is acting parallel to the [100] face. Figure 5(a) and 5(c) is illustrating the geometric configuration of unit cells with respect to the electric field direction and the unit cell length along parallel ( $L_{\parallel}$ ) and perpendicular to the electric field ( $L_{\perp}$ ).[37] In the case when electric field is parallel to the fourfold axis, i.e.,  $E \parallel [100]$ , then we can write

$$L_{\parallel}^2 = L_o^2(1 + 2u_{xx}) \quad (3)$$

Since we assume electric field is along  $x$  direction, Equation (1) could be written as

$$u_{xx} = R_{xxxx}E^2 = R_1E^2 \quad (4)$$

$$L_{\parallel}^2 = L_o^2(1 + 2R_1E^2) \quad (5)$$

We have taken the value of  $R_1 = -1.766 \times 10^{-15} \text{m}^2/\text{V}^2$ . [37] Putting this value into Equation (4) for 0, 5 and 15 V we have obtained relative strain  $(L_{\parallel}^2 - L_o^2)/L_o^2$  and plotted with respect to electric field

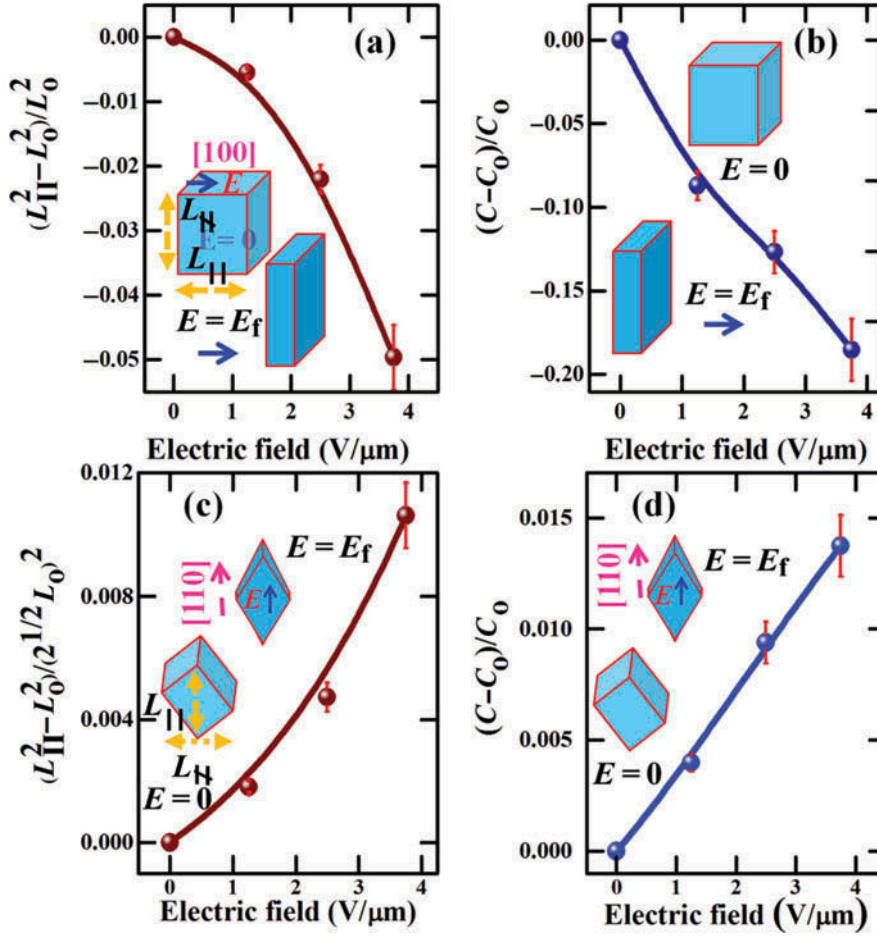


Figure 5. (colour online) Schematic diagram of the electro-active deformation of the unit cell of BPI with increasing electric field: (a) cube at zero electric field and finite electric field ( $E_f$ ) depicting the deformation dynamics when the unit cell dimension shrinks along the electric field, (b) the corresponding capacitance change associated with shrinkage of the unit cell in (a), (c) the electro-active deformation dynamics for the expansion of unit cell dimension along the electric field, (d) the corresponding capacitance change associated with expansion of the unit cell in (c).

in Figure 5(a). It is clear that  $(L_{||}^2 - L_0^2)/L_0^2$  decreases with increasing electric field. We have also plotted the capacitance with electric field at  $64^\circ\text{C}$  (Figure 5(b)) which also shows same decreasing tendency with electric field. From the inset schematics we have tried to give a glimpse, although our sample has a positive dielectric anisotropy the unit cell shrinks along the field direction in both the cases. On the other hand when the applied electric field is parallel to the two-fold axis (e.g.,  $E \parallel [110]$ ) then we can write

$$L_{||}^2 = L_0^2(2 + 2u_{xx} + 2u_{yy} + 4u_{xy}) \quad (6)$$

Electric field will be  $E = \left(\frac{E}{\sqrt{2}}, \frac{E}{\sqrt{2}}, 0\right)$  and

$$u_{xy} = R_{xyxy}E_xE_y = \frac{1}{2}R_3\frac{E^2}{2} \quad (7)$$

$$\frac{(L_{||}^2 - L_0^2)}{L_0^2} = (2 + 2R_1E^2 + 2R_2E^2 + R_3E^2)E^2 \quad (8)$$

Putting the typical values [32] of  $R_1 = -1.766 \times 10^{-15}\text{m}^2/\text{V}^2$ ,  $R_2 = 0.884 \times 10^{-15}\text{m}^2/\text{V}^2$  and  $R_3 = 1.26 \times 10^{-15}\text{m}^2/\text{V}^2$  in Equation (7) we have plotted the results with respect to the same electric field as the previous one and compared with the experimentally obtained change in capacitance in Figure 5(c) and 5 (d), respectively. Dramatically, we find that capacitance change follows the same trend as deformation of the unit cell dimension along the electric field except capacitance is increasing with electric field, which is due to different crystal orientation in the NST cell with respect to electric field direction. Due to the cubic symmetry the average dielectric constant is an isotropic tensor as represented by the circle in Figure 6(a). When field acts parallel to the (110)

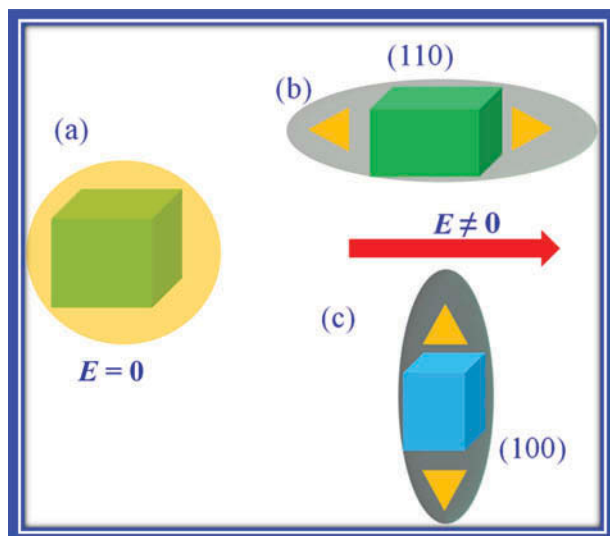


Figure 6. Schematic diagram of (a) cubic unit cell representing dielectrically isotropic, (b) when an electric field is applied parallel to (110) plane, elongated cube acts as rod-like NLC molecule with dielectric anisotropy larger than zero ( $\Delta\epsilon > 0$ ) however (c) when an electric field is applied along (100) plane, cubes with fourfold axis then dilates and acts as rodlike NLC molecule with dielectric anisotropy smaller than zero ( $\Delta\epsilon < 0$ ).

direction, the deformation of the cubic unit cell took place along the electric field, the resultant dielectric constant is depicted by an ellipsoid in Figure 6(b). The shape anisotropy of the unit cell took place in the direction of the electric field in order to attain minimum energy. We can make an analogy that elongated cube becomes ellipsoid whose major axis aligns along the electric field as rod like NLC ( $\Delta\epsilon > 0$ ) and capacitance increases with electric field as the LC molecules reorient along the electric field due to energy minimisation. On the other hand when electric field acts along (100) direction, cubic unit cell contracts and deforms along the direction perpendicular to the electric field as depicted by Figure 6(c). It is analogous to the NLC with ( $\Delta\epsilon < 0$ ) and capacitance decreases as dielectric anisotropy orients perpendicular to the electric field.

Figure 7(a) and 7(b) shows  $V$ - $T$  curves with ascending and descending voltages for NST and ST cell, respectively. We have defined the hysteresis from the voltage difference at 50% of the maximum transmission level ( $\Delta V_{50}$ ). For the NST hysteresis at 20, 30 and 40 are 1.5, 6.8, and 7.8, respectively, whereas ST cell are 0.95, 3.3 and 5.1, respectively. Hysteresis has been reduced dramatically to almost half compared to NST cell and at each voltage. The reason for the less hysteresis in the rubbed cell seems to be due to orientation of the cubes. It is also important to optimise the hysteresis and the driving voltage. If one can avoid the overdriving

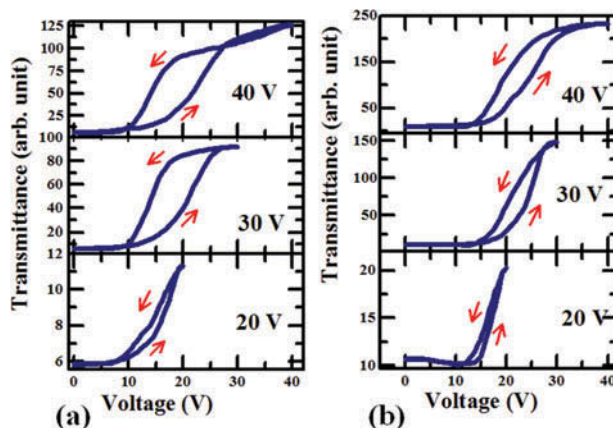


Figure 7.  $V$ - $T$  curves of the IPS cell with different voltage amplitudes: (a) NST and (b) ST. The hysteresis increases with voltage amplitudes in both cells but hysteresis is small in ST cell for all voltages compared to NST cell.

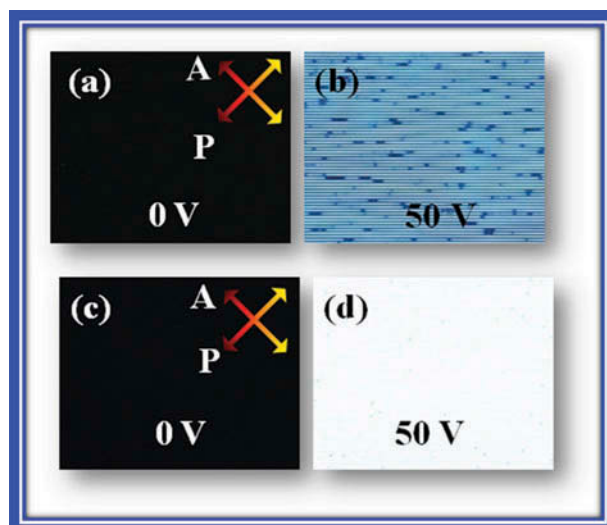


Figure 8. POM texture: (a) NST cell at 0 V, (b) NST cell at 50 V, (c) ST cell at 0 V, (d) ST cell at 50 V.

then hysteresis might be reasonable. The calculated contrast ratio for the NST and ST cell are  $\sim 21$  and  $43$ , respectively, indicating higher contrast ratio can be achieved in the uniformly oriented cubes. The textures at 0 and 50 V of both the cells are shown in Figure 8. We have found out one of the solutions for the high contrast ratio in BPLCDs which has remained unclear.

#### 4. Conclusions

In conclusion, we have found that surface treatment of the BPLC cell can tune the arrangement of the unit cells and reduce hysteresis significantly. The

mismatching of the unit cells seems to be partly responsible for hysteresis and poor contrast ratio. The uniform arrangement of cubes also increases the transmission intensity and it has better ability to withstand electrostriction. The proposed unique capacitive technique could be useful for detection of normal and anomalous electrostriction and different phases with varying temperature. Temperature-dependent capacitance can help to detect the transition of different phases of BPs under in situ and in-plane cell.

#### Disclosure statement

No potential conflict of interest was reported by the authors.

#### Funding

This research was supported by the Basic Science Research Program and BK Plus through the National Research Foundation of Korea (NRF) funded by the Ministry of Education [grant number 2013R1A1A2005630].

#### References

- [1] Kitzerow H-S. Blue phases at work! *Chem Phys Chem*. 2006;7:63–66.
- [2] Meiboom S, Sammon M, Berreman DW. Lattice symmetry of the cholesteric blue phases. *Phys Rev A*. 1983;28:3553–3560. doi:10.1103/PhysRevA.28.3553.
- [3] Crooker PP. Plenary lecture the blue phases a review of experiments. *Liq Cryst*. 1989;5:751–775. doi:10.1080/02678298908026383.
- [4] Keyes PH. High-chirality blue-phase lattices are unstable: a theory for the formation of blue phase III. *Phys Rev Lett*. 1990;65:436–439. doi:10.1103/PhysRevLett.65.436.
- [5] Hornreich RM, Kugler M, Shtrikman S. Localized instabilities and the order-disorder transition in cholesteric liquid crystals. *Phys Rev Lett*. 1982;48:1404–1407. doi:10.1103/PhysRevLett.48.1404.
- [6] Henrich O, Stratford K, Cates ME, Marenduzzo D. Structure of blue phase III of cholesteric liquid crystals. *Phys Rev Lett*. 2011;106:107801. doi:10.1103/PhysRevLett.106.107801.
- [7] Chen Y, Yan J, Sun J, Wu S-T, Liang X, Liu S-H, Hsieh P-J, Cheng K-L, Shiu J-W. A microsecond-response polymer-stabilized blue phase liquid crystal. *Appl Phys Lett*. 2011;99:201105. doi:10.1063/1.3662391.
- [8] Chen K-M, Gauza S, Xianyu HQ, Wu S-T. Submillisecond gray-level response time of a polymer-stabilized blue-phase liquid crystal. *J Display Technol*. 2010;6:49–51. doi:10.1109/JDT.2009.2037981.
- [9] Ge Z, Rao L, Gauza S, Wu S-T. Modeling of blue phase liquid crystal displays. *J Display Technol*. 2009;5:250–256. doi:10.1109/JDT.2009.2022849.
- [10] Kikuchi H, Yokota M, Hisakado Y, Yang H, Kajiyama T. Polymer-stabilized liquid crystal blue phases. *Nat Mater*. 2002;1:64–68. doi:10.1038/nmat712.
- [11] Castles F, Day FV, Morris SM, Ko D-H, Gardiner DJ, Qasim MM, Nosheen S, Hands PJW, Choi SS, Friend RH, Coles HJ. Blue-phase templated fabrication of three-dimensional nanostructures for photonic applications. *Nat Mater*. 2012;11:599–603. doi:10.1038/nmat3330.
- [12] Yoshida H, Tanaka Y, Kawamoto K, Kubo H, Tsuda T, Fujii A, Kuwabata S, Kikuchi H, Ozaki M. Nanoparticle-stabilized cholesteric blue phases. *Appl Phys Express*. 2009;2:121501. doi:10.1143/APEX.2.121501.
- [13] Karatairi E, Rožič B, Kutnjak Z, Tzitzios V, Nounesis G, Cordoyiannis G, Thoen J, Glorieux C, Kralj S. Nanoparticle-induced widening of the temperature range of liquid-crystalline blue phases. *Phys Rev E*. 2010;81:041703. doi:10.1103/PhysRevE.81.041703.
- [14] Cordoyiannis G, Losada-Pérez P, Tripathi CSP, Rožič B, Tkalec U, Tzitzios V, Karatairi E, Nounesis G, Kutnjak Z, Mušević I, Glorieux C, Kralj S, Thoen J. Blue phase III widening in CE6-dispersed surface-functionalized CdSe nanoparticles. *Liq Cryst*. 2010;37:1419–1426. doi:10.1080/02678292.2010.519057.
- [15] Nayek P, Mukherjee A, Jeong H, Kang S-W, Lee SH, Yokoyama H. Phase behavior and thermal stabilization study of blue phase liquid crystal-unfunctionalized nanoparticle blends. *Nanosci Nanotechnol*. 2013;13:4072–4078. doi:10.1166/jnn.2013.6687.
- [16] He WL, Pan GH, Yang Z, Zhao DY, Niu GG, Huang W, Yuan XT, Guo JB, Cao H, Yang H. Wide blue phase range in a Hydrogen-bonded self-assembled complex of chiral fluoro-substituted benzoic acid and pyridine derivative. *Adv Mater*. 2009;21:2050–2053. doi:10.1002/adma.200802927.
- [17] Coles HJ, Pivnenko MN. Liquid crystal ‘blue phases’ with a wide temperature range. *Nature*. 2005;436:997–1000. doi:10.1038/nature03932.
- [18] Rao LH, Ge ZB, Wu S-T, Lee SH. Low voltage blue-phase liquid crystal displays. *Appl Phys Lett*. 2009;95:231101. doi:10.1063/1.3271771.
- [19] Kim MY, Kim MS, Kang BG, Kim M-K, Yoon SI, Lee SH, Ge ZB, Rao LH, Gauza S, Wu S-T. Wall-shaped electrodes for reducing the operation voltage of polymer-stabilized blue phase liquid crystal displays. *J Phys D: Appl Phys*. 2009;42:235502. doi:10.1088/0022-3727/42/23/235502.
- [20] Rao LH, Yan J, Wu S-T, Yamamoto S-I, Haseba Y. A large kerr constant polymer-stabilized blue phase liquid crystal. *Appl Phys Lett*. 2011;98:081109. doi:10.1063/1.3559614.
- [21] Yoon SI, Yang GH, Nayek P, Jeong H, Lee SH, Hong SH, Lee HJ, Shin S-T. Study on the light leakage mechanism of a blue phase liquid crystal cell with oblique interfaces. *J Phys D: Appl Phys*. 2012;45:105304. doi:10.1088/0022-3727/45/10/105304.
- [22] Chen K-M, Gauza S, Xianyu HQ, Wu S-T. Hysteresis effects in blue-phase liquid crystals. *J Disp Technol*. 2010;6:318–322. doi:10.1109/JDT.2010.2055039.
- [23] Mukherjee A, Yang GH, Jeong H, Nayek P, Kang S-W, Lee SH, Hong SH, Lee HJ, Shin S-T. Emergence of a novel optically isotropic transient state with low frequency in a blue phase liquid crystal mixture. *Liq Cryst*. 2012;39:231–237. doi:10.1080/02678292.2011.631045.
- [24] Nayek P, Jeong H, Kang S-W, Lee SH, Park H-S, Lee HJ, Kim HS, Lee G-D. Effect of the grain size on

- hysteresis of liquid-crystalline blue phase I. *J Soc Inf Display*. 2012;20:318. doi:10.1889/JSID20.6.318.
- [25] Nayek P, Jeong H, Park HR, Kang S-W, Lee SH, Park HS, Lee HJ, Kim HS. Tailoring monodomain in blue phase liquid crystal by surface pinning effect. *Appl Phys Express*. 2012;5:051701. doi:10.1143/APEX.5.051701.
- [26] Pieranski P, Dubois-Violette E, Rothen F, Strzelecki L. Geometry of Kossel lines in colloidal crystals. *J Physique*. 1981;42:53–60. doi:10.1051/jphys:0198100420105300.
- [27] Miller RJ, Gleeson HF. Lattice parameter measurements from the Kossel diagrams of the cubic liquid crystal blue phases. *J Phys II France*. 1996;6:909–922. doi:10.1051/jp2:1996219.
- [28] Wang C-T, Liu H-Y, Cheng -H-H, Lin T-H. Bistable effect in the liquid crystal blue phase. *Appl Phys Lett*. 2010;96:041106. doi:10.1063/1.3293302.
- [29] Heppke G, Jérôme B, Kitzerow H-S, Pieranski P. Electrostriction of the cholesteric blue phases BPI and BPII in mixtures with positive dielectric anisotropy. *J Phys*. 1989;50:2991–2998. doi:10.1051/jphys:0198900500190299100.
- [30] Cladis PE, Garel T, Pieranski P. Kossel diagrams show electric-field-induced cubic-tetragonal structural transition in frustrated liquid-crystal blue phases. *Phys Rev Lett*. 1986;57:2841–2844. doi:10.1103/PhysRevLett.57.2841.
- [31] Tone H, Yoshida H, Yabu S, Ozaki M, Kikuchi H. Effect of anisotropic lattice deformation on the Kerr coefficient of polymer-stabilized blue-phase liquid crystals. *Phys Rev E*. 2014;89:012506. doi:10.1103/PhysRevE.89.012506.
- [32] Pierański P, Cladis PE, Garel T, Barbet-Massin R. Orientation of crystals of blue phases by electric fields. *J Phys Paris*. 1986;47:139–143. doi:10.1051/jphys:01986004701013900.
- [33] Tiribocchi A, Gonnella G, Marenduzzo D, Orlandini E. Switching dynamics in cholesteric blue phases. *Soft Matter*. 2011;7:3295–3306. doi:10.1039/c0sm00979b.
- [34] Stark H, Trebin H-R. Theory of electrostriction of liquid-crystalline blue phases I and II. *Phys Rev A*. 1991;44:2752–2755. doi:10.1103/PhysRevA.44.2752.
- [35] Porsch F, Stegemeyer H. Electrostriction of liquid crystalline blue phases. *Chem Phys Lett*. 1989;155:620–623. doi:10.1016/0009-2614(89)87484-6.
- [36] Alexander GP, Marenduzzo D. Cubic blue phases in electric fields. *Europhys Lett*. 2008;81:66004. doi:10.1209/0295-5075/81/66004.
- [37] Fukuda J-I, Yoneya M, Yokoyama H. Simulation of cholesteric blue phases using a Landau-de Gennes theory: effect of an applied electric field. *Phys Rev E*. 2009;80:031706. doi:10.1103/PhysRevE.80.031706.